Author(s): Volbach, Lucia; Struch, Niklas; Bohle, Fabian; Topic, Filip; Schnakenburg, Gregor;
Schneider, Andreas; Rissanen, Kari; Grimme, Stefan; Lützen, Arne

Title: Influencing the self-sorting behavior of [2.2]paracyclophane based ligands by
introducing isostructural binding motifs

Year: 2020

Version: Accepted version (Final draft)

Please cite the original version:

Volbach, L., Struch, N., Bohle, F., Topic, F., Schnakenburg, G., Schneider, A., Rissanen, K.,
Grimme, S., & Lützen, A. (2020). Influencing the self-sorting behavior of [2.2]paracyclophane
based ligands by introducing isostructural binding motifs. Chemistry : A European Journal,
26(15), 3335-3347. https://doi.org/10.1002/chem.201905070

Influencing the Self-Sorting Behavior of [2.2]Paracyclophane-Based Ligands by Introducing Isostructural Binding Motifs

Lucia Volbach,[a] Niklas Struch,[a, b] Fabian Bohle,[c] Filip Topić,[d, e] Gregor Schnakenburg,[f] Andreas Schneider,[a] Kari Rissanen,[d] Stefan Grimme,[c] and Arne Lützen*[a]

Abstract: Two isostructural ligands with either nitrile (L^{nit}) or isonitrile (L^{iso}) moieties directly connected to a [2.2]paracyclophane backbone with pseudo-*meta* substitution pattern have been synthesized. The ligand itself (L^{nit}) or its precursors (L^{iso}) were resolved by HPLC on a chiral stationary phase and the absolute configuration of the isolated enantiomers was assigned by XRD analysis and/or by comparison of quantum-chemical simulated and experimental electronic circular dichroism (ECD) spectra. Surprisingly, the resulting metallosupramolecular aggregates formed in solution upon coordination of [(dppp)Pd(OTf)$_2$] differ in their composition: whereas L^{nit} forms dinuclear complexes, L^{iso} exclusively forms trinuclear ones. Furthermore, they also differ in their chiral self-sorting behavior as (*rac*)-L^{iso} undergoes exclusive social self-sorting leading to a heterochiral assembly, whereas (*rac*)-L^{iso} shows a twofold preference for the formation of homochiral complexes in a narcissistic self-sorting manner as proven by ESI mass spectrometry and NMR spectroscopy. Interestingly, upon crystallization, these discrete aggregates undergo structural transformation to coordination polymers, as evidenced by single-crystal X-ray diffraction.

Introduction

Mastering the self-sorting behavior in multicomponent mixtures is of utmost importance to cope with the immense structural complexity that such systems offer.[1] Geometrical (self-)complementarity concerning shape and size but also chirality

[a] Dr. L. Volbach, Dr. N. Struch, A. Schneider, Prof. Dr. A. Lützen
Kekulé-Institute of Organic Chemistry and Biochemistry
University of Bonn
Gerhard-Domagk Strasse 1, 53121 Bonn (Germany)
E-mail: arne.luetzen@uni-bonn.de

[b] Dr. N. Struch
current address: Arlanxeo Netherlands B.V.
Urmonderbaan 24, 6167 RD Geleen (The Netherlands)

[c] F. Bohle, Prof. Dr. S. Grimme
Mulliken Center for Theoretical Chemistry, University of Bonn
Beringstrasse 4, 53115 Bonn (Germany)

[d] Dr. F. Topić, Prof. Dr. K. Rissanen
Department of Chemistry, University of Jyväskylä
P.O. Box 35, 40014 Jyväskylä (Finland)

[e] Dr. F. Topić
current address: Department of Chemistry, McGill University
801 Sherbrooke St. West, Montreal, Qc H3A 0B8 (Canada)

[f] Dr. G. Schnakenburg
Institute of Inorganic Chemistry, University of Bonn
Gerhard-Domagk Strasse 1, 53121 Bonn (Germany)

Supporting information and the ORCID identification number(s) for the author(s) of this article can be found under:
https://doi.org/10.1002/chem.201905070.

have been used to achieve self-sorting either in a narcissistic[2] (also known as self-recognition[3]) or social[4] (also called self-discrimination[5]) manner. Among the features mentioned above, high-fidelity self-sorting is most challenging with enantiomers that are usually highly similar competitors due to their equal size and shape and the chirality as the only difference. Although successful chiral self-sorting is well established in the solid state due to strong interactions and cooperative binding mechanisms found in crystalline matter,[6] self-sorting of racemic mixtures in solution is still a true challenge.[7] Nevertheless, both scenarios, the heterochiral social[5, 8, 9] and the homochiral narcissistic self-sorting[10, 11] have been reported in metallosupramolecular chemistry. These studies revealed that there are several possibilities to affect and fine-tune the self-sorting behavior, for example, by varying the overall size, the opening angle and the steric bulk of bridging rigid V-shaped ligands.

Based on structural findings in those studies, we wanted to introduce yet another variable concerning only the metal binding unit, to get further insight into these processes and factors that might rule their outcome. Herein, we report on the comparison of two different coordination motifs with regard to self-sorting by introducing two ligands with equal size, shape and coordination angles. The ligands are designed to form supramolecular architectures in solution and in the solid state upon coordination to *cis*-protected palladium(II)-ions,[12] giving rise to [(dppp)$_n$M$_n$L$_n$] complexes, which have been proven a simple, yet successful, platform for investigating changes in the self-sorting behavior.

Results and Discussion

The design is based on an analogy to a *meta*-substituted benzene core furnished with the commonly used 4-pyridyl moiety. In the literature, there are several examples for directly bound and elongated ligands with for example, ethynyl-spacers coordinating to palladium(II).[13] To study chiral self-sorting behavior, we decided to use a pseudo-*meta*-substituted [2.2]paracyclophane backbone as a chiral substitute for the central *meta*-functionalized benzene ring, which also arranges its functional groups at an angle of about 120° designed to construct discrete coordination architectures. Additionally, this scaffold comes with some adaptability due to a possible twist of approximately 12° between the aromatic decks.[14] Considering that we wanted to study two different ligands with essentially equal size and shape, we decided to use nitrile and isonitrile groups (bond length of the CN bond in nitriles 1.5 Å and in isonitriles 1.7 Å, respectively),[15] which are formally isoelectronic to carbon monoxide and have been employed previously to construct metallosupramolecular architectures.[9f, 16] It is worth mentioning, though, that multitopic oligoisonitrile ligands have—to the best of our knowledge—not been used for the self-assembly of discrete cyclic or cage-like metallosupramolecular aggregates so far. Both nitriles and isonitriles represent very slim metal-binding motifs. However, they differ in the relative strength of the metal–ligand interaction because the isonitriles bind—similarly to pyridines—much stronger to metal ions like palladium(II) ions than the corresponding nitriles.[17]

For our purpose, we synthesized two ligands with either two nitrile or isonitrile moieties attached directly to the [2.2]paracyclophane backbone in a pseudo-*meta*-4,15-substitution pattern. This orientates the functional groups at an angle of about 120° and positions the binding sites spatially close to the planar chiral center, a design intended to give rise to discrete coordination architectures and enable the study of the influence of binding strength on self-sorting.

Synthesis

The synthesis of the two different ligands **L**[nit] and **L**[iso] (Scheme 1) started with the commercially available unsubstituted [2.2]paracyclophane **1** (Scheme 2) which can be easily functionalized through the bromination method developed by Hopf et al. to yield 4,15-dibromo[2.2]-paracyclophane **2** and its achiral regioisomer 4,16-dibromo-[2.2]paracyclophane, which could be separated by recrystallization.[18]
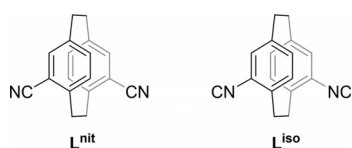
Scheme 1. Pseudo-*meta* functionalized [2.2]paracyclophane ligands **L**[nit] and **L**[iso].
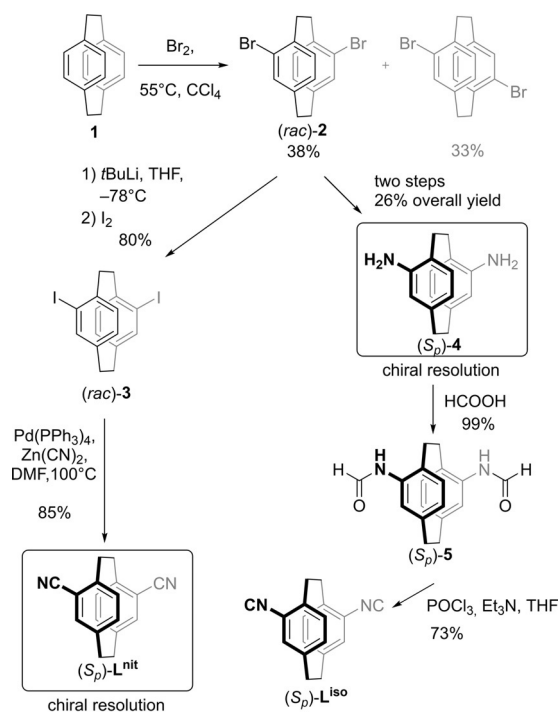
Scheme 2. Synthesis of ligands **L**[nit] and **L**[iso].

The synthesis of the racemic ligand **L**[nit] was already reported by Cram and co-workers in 1975[19] but it has neither been chirally resolved nor used for metal-complexation studies so far.

We obtained the ligand **L**[nit] by an alternative route achieving higher yields. Specifically, we performed the already reported bromine–lithium exchange in THF at −78 °C first by using *t*BuLi and then by quenching the dilithiated species with iodine to access the diiodinated [2.2]paracyclophane **3** in 80 % yield.[20] Next, we synthesized **L**[nit] by palladium-catalyzed cyanation reaction providing the desired product in 85 % yield.

Considering that we needed both the racemic and the enantiomerically pure compounds for our studies, we next resolved ligand **L**[nit] by HPLC on a Chiralpak IB stationary phase both on the analytical and semi-preparative scale (see Supporting Information). The absolute configuration could be elucidated by comparison of experimentally recorded CD spectra of the resolved material with theoretically simulated ones obtained from simplified time-dependent (sTD)-DFT-calculations.[21] This assignment was corroborated by determination of the Flack parameter by single crystal X-ray diffraction and subsequent analysis of the Bijvoet differences by using Bayesian statistics (vide infra).[22] Both techniques proved that the (*R*p)-enantiomer was the first to elute (see Supporting Information).

The new ligand **L**[iso] was obtained in a two-step synthesis with excellent yields by using the previously reported pseudo-*meta*-4,15-diamino[2.2]paracyclophane[20] **4** as the starting material. First, the 4,15-diformamido[2.2]paracyclophane **5** was obtained by dissolving the starting material in an excess of formic acid and sonicating the solution in an ultrasonic bath for 6 h. After purification by filtration through a short silica column and treatment with POCl₃ in a 1:1 mixture of THF and triethylamine, ligand **L**[iso] was obtained in 73 % yield. Fortunate-

ly, pseudo-*meta*-4,15-diamino[2.2]paracyclophane **4** is available in enantiomerically pure form, because all attempts to resolve ligand **L^iso** directly by HPLC using chiral columns in a sufficient manner with regard to enantiomeric purity failed. Nevertheless, the absolute configuration of the resolved enantiomers could be confirmed by single crystal X-ray diffraction and subsequent analysis of the Bijvoet differences by using Bayesian statistics (vide infra and Supporting Information).[22]

In this way, we had access to both ligands in racemic and optically pure form, which allowed us to compare their self-sorting behavior in the self-assembly of metallosupramolecular complexes upon coordination to *cis*-protected palladium(II) ions in solution and in the solid state.

Coordination studies: solution and gas-phase studies

The metallosupramolecular aggregates were formed upon mixing stoichiometric amounts of ligand (each either in racemic or enantiomerically pure form) with [(dppp)Pd(OTf$_2$)][23] in different solvents and characterized by NMR techniques and, where possible, by ESI-MS measurements.

Coordination of ligand **L^nit** can be observed in, for example, nitromethane. The ^{1}H NMR spectrum of the complex formed from enantiomerically pure ligand **L^nit** shows only one set of sharp, significantly shifted signals, indicating the successful formation of a single discrete homochiral metallosupramolecular aggregate of D_2 symmetry (Figure 1).
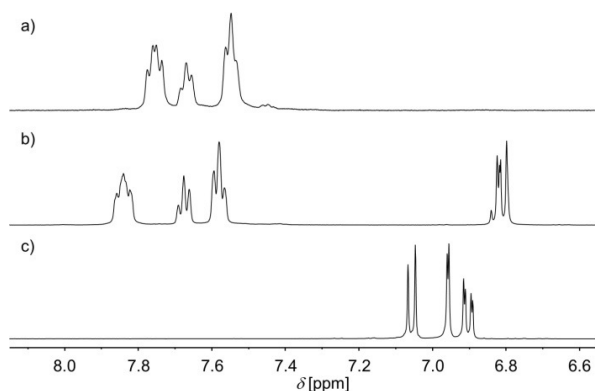
Figure 2. ^{1}H DOSY NMR Spectra (499 MHz in CD$_3$NO$_2$ at 293 K) of the aggregate obtained from a 1:1 mixture of [(dppp)Pd(OTf)$_2$] and (S_p)-**L^nit**.

binding between the palladium atoms and the nitrogen donors.

Nevertheless, we went on to analyze the behavior of the racemic ligand (*rac*)-**L^nit** by recording a similar set of NMR experiments. Comparing them with the spectra of the free ligand and the homochiral complex formed from the optically pure ligand revealed that a single metallosupramolecular complex is formed which is different from the homochiral dinuclear complex as indicated by significant shifts (Figure 3).

Figure 1. ^{1}H NMR (499 MHz in CD$_3$NO$_2$ at 298 K) of a) [(dppp)Pd(OTf)$_2$], b) a 1:1 mixture of [(dppp)Pd(OTf)$_2$] and (S_p)-**L^nit**, and c) ligand **L^nit**.
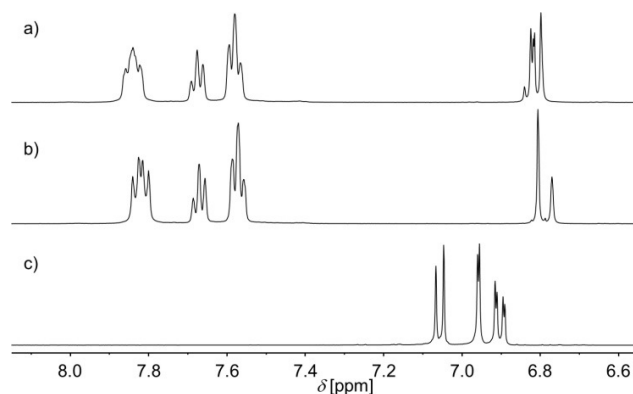
Figure 3. ^{1}H NMR (499 MHz in CD$_3$NO$_2$ at 298 K) of a) 1:1 mixture of [(dppp)Pd(OTf)$_2$] and (S_p)-**L^nit**, b) a 1:1 mixture of [(dppp)Pd(OTf)$_2$] and (*rac*)-**L^nit**, and c) ligand **L^nit**.

Further proof of the exclusive formation of only one aggregate was obtained by ^{1}H DOSY experiments (Figure 2): all signals belong to a single species with a diffusion coefficient $D = 4.42 \times 10^{-6}$ cm^{2}s^{-1}, which translates to a hydrodynamic diameter $d = 16.0$ Å, according to the Stokes–Einstein equation. This is considerably larger than the ligand **L^nit** alone, but matches very well the calculated value[24] of the hydrodynamic diameter of a dinuclear rhomb (about 16 Å, see Figure 4a).

Unfortunately, despite our best efforts, we have not been able to obtain any mass spectra of this kind of complexes formed from bis(nitrile) ligands, presumably due to the weak
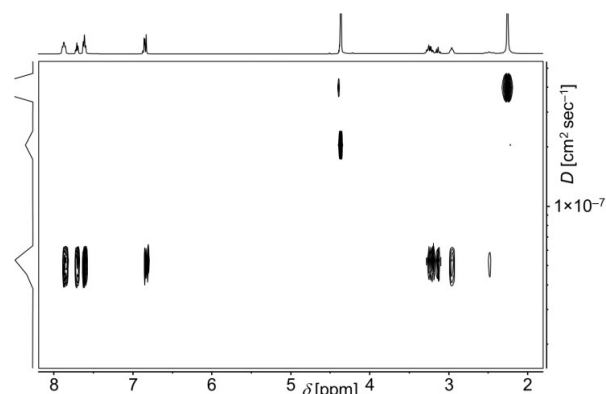
Considering that the ^{1}H DOSY experiment (see Supporting Information) again indicate the formation of a dinuclear assembly, we conclude that the self-assembly process involving (*rac*)-**L^nit** is still highly diastereoselective, but results in the exclusive formation of the heterochiral C_{2v} symmetric complex (Figure 4b).

This interpretation in favor of a diastereoselective self-sorting in a self-discriminating manner was further corroborated by comparison of ^{31}P NMR spectra, which show a single signal in each case (see Supporting Information). Compared to [(dppp)Pd(OTf)$_2$], the signals of both the homochiral [(dppp)$_2$Pd$_2$\{(S_p)-**L^nit**\}$_2$](OTf)$_4$ and the heterochiral

a)

R_p

R_p

[(dppp)₂Pd₂{(R_p)-$\mathbf{L^{nit}}$}₂]⁴⁺

b)

S_p

R_p

[(dppp)₂Pd₂{(S_p)-$\mathbf{L^{nit}}$} {(R_p)-$\mathbf{L^{nit}}$}]⁴⁺

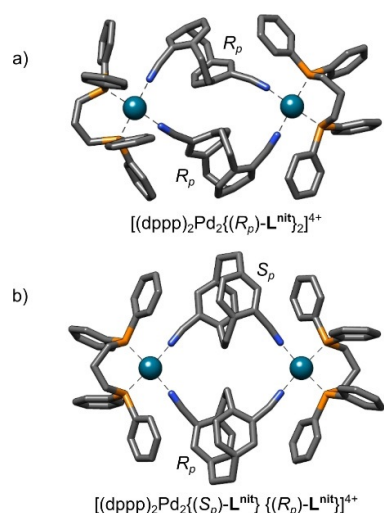**Figure 4.** PBEh-3c/DCOSMO-RS(NO₂CH₃) optimized structures of the cationic units of dinuclear metallosupramolecular rhombs: a) homochiral [(dppp)₂Pd₂{(R_p)-$\mathbf{L^{nit}}$}₂](OTf)₄ and b) heterochiral [(dppp)₂Pd₂{(S_p)-$\mathbf{L^{nit}}$}{(R_p)-$\mathbf{L^{nit}}$}](OTf)₄ (hydrogen atoms are omitted, color scheme: carbon–grey, nitrogen–blue, phosphorous–orange, palladium–petrol, see Supporting Information for further details).

[(dppp)₂Pd₂{(S_p)-$\mathbf{L^{nit}}$}{(R_p)-$\mathbf{L^{nit}}$}](OTf)₄ are high-field shifted, indicating the selective formation of the desired dinuclear metallosupramolecular aggregates. However, the ³¹P signals differ in such a way that the signal observed for the heterochiral complex is shifted even further to high field compared to that of its homochiral stereoisomer.

This difference is not a result of an anion template effect because the signals of the triflate anions in the ¹⁹F NMR spectra were found at the same shift for both dinuclear aggregates [(dppp)₂Pd₂{(S_p)-$\mathbf{L^{nit}}$}₂](OTf)₄ and [(dppp)₂Pd₂{(S_p)-$\mathbf{L^{nit}}$}{(R_p)-

$\mathbf{L^{nit}}$}](OTf)₄, although being clearly different from that of the starting material [(dppp)Pd(OTf)₂] (see Supporting Information).

To complete these studies, it is important to mention that essentially the same behavior was observed when chlorinated solvents like dichloromethane were used, but acetonitrile and acetone both proved to be too competitive as they (expectedly) prohibited the complexation (see Supporting Information).[25]

Having established the highly diastereoselective self-sorting during the self-assembly of ligand $\mathbf{L^{nit}}$ upon coordination to [(dppp)Pd(OTf)₂], we turned our attention to ligand $\mathbf{L^{iso}}$. Like $\mathbf{L^{nit}}$, enantiomerically pure $\mathbf{L^{iso}}$ also gives rise to a single metallosupramolecular species upon coordination to the *cis*-protected Pd^{II} complex fragment. Surprisingly, however, analysis of the DOSY spectra clearly indicate that the aggregate formed from enantiomerically pure $\mathbf{L^{iso}}$ has a diameter of $d = 22.6$ Å, thus being considerably larger than the dinuclear homochiral complex obtained by self-assembly of optically pure $\mathbf{L^{nit}}$ and [(dppp)Pd(OTf)₂] (see Supporting Information).

Fortunately, complexes of palladium(II) ions and isonitrile ligands are more stable than their nitrile analogues,[17] and hence, can be studied by ESI-MS (Figure 5). These studies confirm the formation of trinuclear complexes with enantiomerically pure and racemic $\mathbf{L^{iso}}$, as indicated by signals at $m/z = 1463.2$ which can be assigned to {[(dppp)₃Pd₃($\mathbf{L^{iso}}$)₃](OTf)₄}²⁺, or the signals at $m/z = 811.2$ and 925.1 which can both be assigned to superimposed signals arising from triply charged ions {[(dppp)₃Pd₃($\mathbf{L^{iso}}$)₃](Cl)₃}³⁺ and {[(dppp)₃Pd₃($\mathbf{L^{iso}}$)₃](OTf)₃}³⁺ and their singly charged fragments {[(dppp)Pd($\mathbf{L^{iso}}$)](X)}⁺ (X = Cl or OTf), respectively.[26]

Hence, we can conclude that the enantiomerically pure ligand $\mathbf{L^{iso}}$ successfully forms a discrete homochiral trinuclear metallosupramolecular aggregate of D_3 symmetry upon coordination to [(dppp)Pd(OTf)₂].
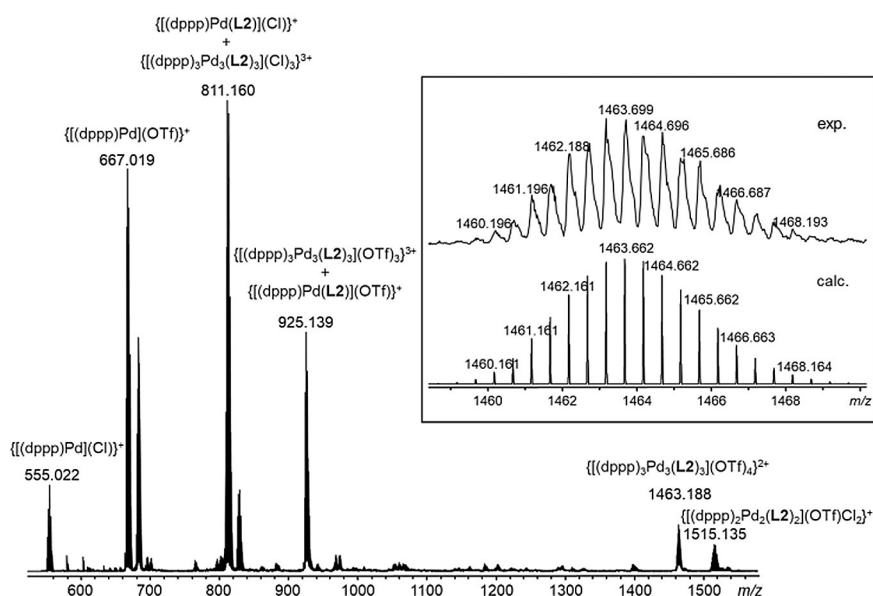

Figure 5. Positive ESI-MS spectrum of the 1:1 mixture of [(dppp)Pd(OTf)₂] and (*rac*)-$\mathbf{L^{iso}}$ showing signals of trinuclear 3:3 aggregates and their fragments. The inset shows the comparison of the experimentally determined isotope pattern of the {[(dppp)₃Pd₃($\mathbf{L^{iso}}$)₃](OTf)₄}²⁺ ion and the calculated one.
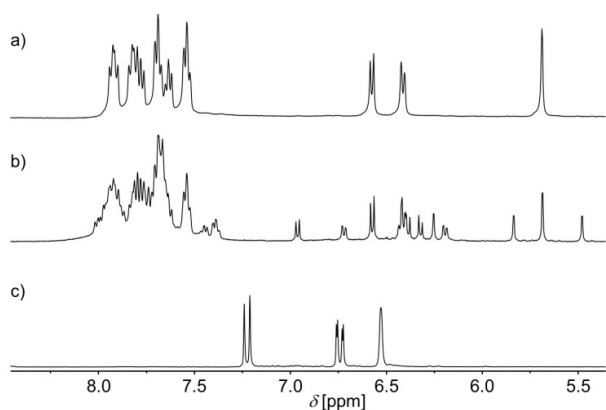
Figure 6. ^{1}H NMR (499 MHz in CD$_3$NO$_2$ at 293 K) of a) [(dppp)$_3$Pd$_3${(S_p)-L^{iso}}$_3$]OTf$_6$, b) the complexes formed from a 1:1 mixture of [(dppp)Pd(OTf)$_2$] and (*rac*)-L^{iso}, and c) ligand (*rac*)-L^{iso}.

Next, we turned our attention to (*rac*)-L^{iso}. Considering that ESI-MS already revealed the formation of trinuclear complexes, NMR spectroscopic experiments were performed to study its chiral self-sorting behavior. Interestingly, the ^{1}H NMR spectrum of a 1:1 mixture of [(dppp)Pd(OTf)$_2$] and (*rac*)-L^{iso} in [D$_3$]nitromethane looks rather complicated (Figure 6).

2D-Correlated spectra confirmed the formation of two different species and ^{1}H DOSY experiments nicely show that these are both of very similar size giving rise to a diffusion coefficient $D = 3.20 \times 10^{-6}$ cm^2 s^{-1}. This value is again considerably smaller than that observed for the dinuclear complexes formed from ligand L^{nit} (Figure 7), but nicely matches that of the homochiral trinuclear complex obtained from enantiomerically pure L^{iso}.

Therefore, we can assign the two species formed as the homochiral trinuclear complex [(dppp)$_3$Pd$_3${(S_p)-L^{iso}}$_3$](OTf)$_6$ and its enantiomer, and the heterochiral complex [(dppp)$_3$Pd$_3${(S_p)-L^{iso}}$_2${(R_p)-L^{iso}}](OTf)$_6$ and its enantiomer, respectively (Figure 8).

Figure 8. PBEh-3c/DCOSMO-RS(NO$_2$CH$_3$) optimized structures of the cationic units of trinuclear metallosupramolecular triangles: a) the homochiral [(dppp)$_3$Pd$_3${(R_p)-L^{iso}}$_3$](OTf)$_6$ and b) heterochiral [(dppp)$_3$Pd$_3${(R_p)-L^{iso}}$_2${(S_p)-L^{iso}}](OTf)$_6$ (hydrogen atoms are omitted, color scheme: carbon–grey, nitrogen–blue, phosphorous–orange, palladium–petrol, see Supporting Information for further details).

This is also in agreement with the analysis of the ^{31}P NMR spectra (see Supporting Information). Whereas the homochiral complex [(dppp)$_3$Pd$_3${(S_p)-L^{iso}}$_3$](OTf)$_6$ only gives rise to a single signal that is significantly shifted compared to the signal observed for [(dppp)Pd(OTf)$_2$], the mixture of the racemic homochiral and heterochiral trinuclear complexes gave rise to four signals that are again shifted compared to that of [(dppp)Pd(OTf)$_2$].

Like in the case of L^{nit}, we did not observe any anion template effect during the self-assembly of L^{iso} as we observed only single signals in each of the recorded ^{19}F NMR spectra, which were considerably shifted compared to that of [(dppp)Pd(OTf)$_2$] (see Supporting Information).

Integration of the signals in the ^{1}H and ^{31}P NMR spectra revealed that the homochiral and heterochiral aggregates do not just form statistically in a 1:3 homo-to-heterochiral ratio but rather in a 1 to 1.5 homo-to-heterochiral ratio in an equilibrated solution (see Supporting Information). This translates to a twofold amplified formation of the homochiral assemblies in a narcissistic self-sorting manner.[27] Thus, the bis(isonitrile) ligand L^{iso} does not only show a different behavior regarding the composition of the metallosupramolecular aggregate formed upon self-assembly with [(dppp)Pd(OTf)$_2$], but it also shows a contrary self-sorting behavior compared to its almost isostructural bis(nitrile) analogue L^{nit} (although the self-sorting with L^{iso} is by far not as perfect as with L^{nit}). This feature is truly remarkable, having in mind the close structural similarity of the two ligands. Obviously, though, these two ligands differ in

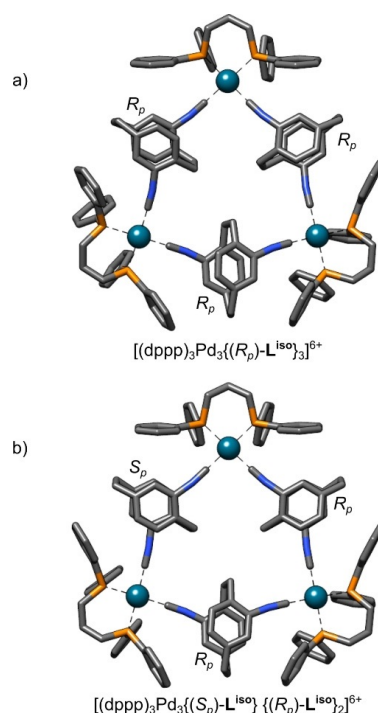**Figure 7.** Superimposed ^{1}H 2D DOSY NMR spectra (499 MHz in CD$_3$NO$_2$ at 298 K) of [(dppp)$_2$Pd$_2${(S_p)-L^{nit}}{(R_p)-L^{nit}}](OTf)$_4$ obtained upon mixing of [(dppp)Pd(OTf)$_2$] and (*rac*)-L^{nit} (black) and the mixture of [(dppp)$_2$Pd$_2${(S_p)-L^{iso}}$_2${(R_p)-L^{iso}}](OTf)$_6$ and the [(dppp)$_2$Pd$_2${(S_p)-L^{iso}}$_3$](OTf)$_6$ and their enantiomers, respectively, obtained upon mixing of [(dppp)Pd(OTf)$_2$] and (*rac*)-L^{iso} (red).

their dipole moments and their binding strength towards palladium, considering that isonitrile ligands generally coordinate to the metal center much more strongly than nitrile ligands due to their better σ-donation and superior π-backbonding ability.[16d,17,28] Consequently, the (M-)N-C-C and (M-)C-N-C bond angles in nitrile and isonitrile complexes, respectively, can differ because the nitriles tend to be linear, whereas considerable bending of isonitrile groups has been reported.[17] This is also reflected by the results of quantum chemical calculations, which were performed on acetonitrile and isocyanomethane, respectively, to estimate the energetic differences of the bending between the two groups (Figure 9).

This might explain the differences in the self-assembly behavior with regard to the different composition, although this needs to be verified with other ligand scaffolds of similar rigidity in the future.
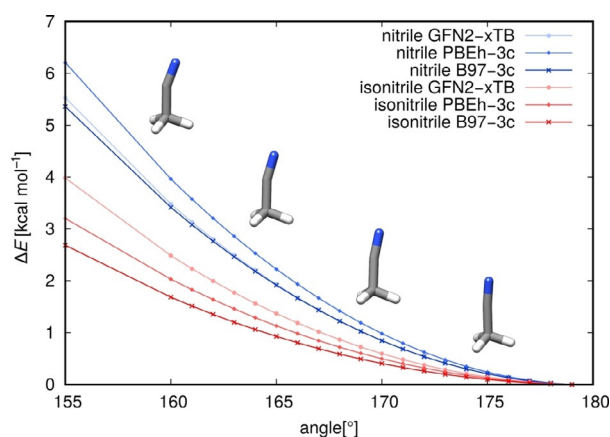

Figure 9. Acetonitrile [N-C-C] and isocyanomethane [C-N-C] bending angle and energy correlation plots obtained when employing different quantum chemical approaches.

A reason for the different self-sorting behavior might be that the heterochiral 2:2 assembly obtained from L^{nit} is very symmetric which might favor its formation. However, the heterochiral 3:3 assembly of L^{iso} is much less symmetric than its homochiral diastereomer, and hence, might be less favored. However, this is only an empirical explanation based on our experience with similar complexes, and hence, should be regarded with great care.

Nevertheless, we performed quantum chemical calculations to get further hints on the reasons for the striking differences of the self-assembly behavior of our two ligands with regard to complex composition because this is the only way to compare the experimentally observed dinuclear palladium(II) complex of L^{nit} with the corresponding hypothetical trinuclear one, and the experimentally observed trinuclear complex of L^{iso} with the hypothetical dinuclear one, respectively.

Thermodynamic data of the tri- and di-nuclear complexes are given in Tables 1 and 2. The semiempirical quantum mechanical GFN2-xTB[34] and high-level PBE0-D4/QZ results show the trinuclear complexes of both binding motifs to be thermodynamically more stable than the dinuclear ones. Considering the efficiency of the GFN2-xTB method compared to the DFT calculations (speed-up of about a factor of 1000 or more), the observed differences in the computed free energies are acceptable and we can recommend this method in general for screening purposes in similar systems, given also that the computed structures are fairly reliable. However, the consistently computed higher stability of trinuclear complexes of L^{nit}, compared to the dinuclear ones, is in stark contrast to the experimental findings. Although the influence of explicit single solvent molecules at the palladium centers was explored in the computations and did not change the initial findings (see Supporting Information), explicit single molecule solvation and implicit solvation models are still inadequate to describe the full

Table 1. Association free energies (ΔG_a) of di- and trinuclear L^{nit} and L^{iso} complexes (all energies and free energies in kcal mol^{-1}).

complex	ΔE (PBE0/def2-QZVP)	ΔE_{disp} (D4)	ΔG_{RRHO} (GFN2-xTB/GBSA (CH$_3$CN))[a]	$\Delta \delta G_{solv}$ (COSMO-RS (NO$_2$CH$_3$))	ΔG_a
[(dppp)$_2$Pd$_2$\{(R_p)-L^{nit}\}$_2$]$^{4+}$	−8.2	−37.5	56.8	−66.0	−54.9
[(dppp)$_3$Pd$_3$\{(R_p)-L^{nit}\}$_3$]$^{6+}$	102.7	−64.8	89.7	−230.3	−102.7
[(dppp)$_2$Pd$_2$\{(R_p)-L^{iso}\}$_2$]$^{4+}$	−41.4	−35.5	60.0	−70.5	−87.4
[(dppp)$_3$Pd$_3$\{(R_p)-L^{iso}\}$_3$]$^{6+}$	44.4	−62.6	93.9	−237.6	−161.9

[a] Acetonitrile was used as solvent, since nitromethane is not parametrized for the implicit solvation model GBSA and the dielectric constant of acetonitrile is very close to that of nitromethane.

Table 2. Free energies of di- and trinuclear L^{nit} and L^{iso} complexes (all energies and free energies in kcal mol^{-1}).

System	ΔG_a (GFN2-xTB/GBSA (CH$_3$CN))[a][c]	$\Delta \Delta G$[b] (2 M$_3$L$_3$−3 M$_2$L$_2$)	ΔG_a (PBE0-D4/def2-QZVP/COSMO-RS(NO$_2$CH$_3$))[a]	$\Delta \Delta G$[b] (2 M$_3$L$_3$−3 M$_2$L$_2$)
[(dppp)$_2$Pd$_2$\{(R_p)-L^{nit}\}$_2$]$^{4+}$	−99.8	−26.3	−54.9	−40.9
[(dppp)$_3$Pd$_3$\{(R_p)-L^{nit}\}$_3$]$^{6+}$	−162.9	−26.3	−102.7	−40.9
[(dppp)$_2$Pd$_2$\{(R_p)-L^{iso}\}$_2$]$^{4+}$	−149.3	−42.8	−87.4	−61.7
[(dppp)$_3$Pd$_3$\{(R_p)-L^{iso}\}$_3$]$^{6+}$	−245.3	−42.8	−161.9	−61.7

[a] ΔG_a association free energies of the complexes. [b] $\Delta \Delta G$ free energy for the reaction 3 M$_2$L$_2$→2 M$_3$L$_3$. [c] Acetonitrile was used as solvent, because nitromethane is not parametrized for the implicit solvation model GBSA and the dielectric constant of acetonitrile is very close to the one of nitromethane.

effect of solvation on the metallosupramolecular aggregates. Obviously, one would have to take into account a whole ensemble of solvent molecules and study its interaction with the dinuclear and trinuclear complexes in order to get the same trend as observed experimentally. Currently, however, this is clearly beyond the boundaries of this theoretical approach. Nevertheless, it is important to note that the trinuclear complex of the isonitrile ligand L^{iso} is not only strongly preferred compared to its potential trinuclear analogue of the nitrile ligand L^{nit}, but it is also much more stabilized compared to the corresponding dinuclear complex as reflected by an energy difference that the solvent effects should not be able to compensate for.

Coordination studies: solid-state studies

We were also able to obtain some single crystals of our ligands (see Supporting Information) and some of their complexes suitable for X-ray analysis. Enantiomerically pure L^{nit} crystallizes in the orthorhombic space group $P2_12_12_1$ upon evaporation of its dichloromethane solution. The absolute configuration assigned by the comparison of experimental and quantum chemically simulated electronic circular dichroism (ECD) spectra could be confirmed by the analysis of the Flack parameter and the Bijvoet differences by using Bayesian statistics derived from the single-crystal XRD analysis of L^{nit} and its coordination complexes. A torsion angle of 119.81° between the two binding units was measured. Enantiomerically pure L^{iso} crystallizes in the same orthorhombic space group $P2_12_12_1$ upon evaporation of solvent from a solution in dichloromethane. As L^{iso} was prepared from enantiomerically pure building blocks **4** its stereochemistry was already known,[20] but the XRD analysis of its single crystals as well as of its coordination complex further confirmed the stereochemical assignment. As anticipated, a dihedral angle of 117.94° between the coordinating isonitrile groups and the centers of the phenyl rings in the paracyclophane backbone was found (vide supra). Hence, the difference in torsion angle between the two ligands amounts to 1.87°.

Diffusion of cyclohexane into a solution of $[(dppp)_2Pd_2\{(R_p)\text{-}L^{nit}\}_2](OTf)_4$ in dichloromethane and subsequent slow evaporation of the solvent afforded single crystals suitable for XRD analysis. Surprisingly, however, addition of the nonpolar solvent and concentration of the solution caused a massive structural rearrangement resulting in a homochiral coordination polymer $[(dppp)Pd\{(R_p)\text{-}L1\}]_n(OTf)_{2n}$ crystallizing in the orthorhombic space group $P2_12_12_1$. The observed polymerization of discrete complexes is most probably due to concentration effects during the crystal growth.[35] Coordination polymers with nitrile ligands are known in literature, but usually contain silver(I) centers.[36] The asymmetric unit of $[(dppp)Pd\{(R_p)\text{-}L^{nit}\}]_n(OTf)_{2n}$ contains one ligand L^{nit}, a dppp-protected palladium ion, two triflate anions and a disordered dichloromethane molecule.

Each metal center is coordinated to one dppp and two ligands L^{nit}, forming a helical coordination polymer. Pd(dppp) moieties form the outer edges while the paracyclophane ligands form the inner core of the coordination polymer
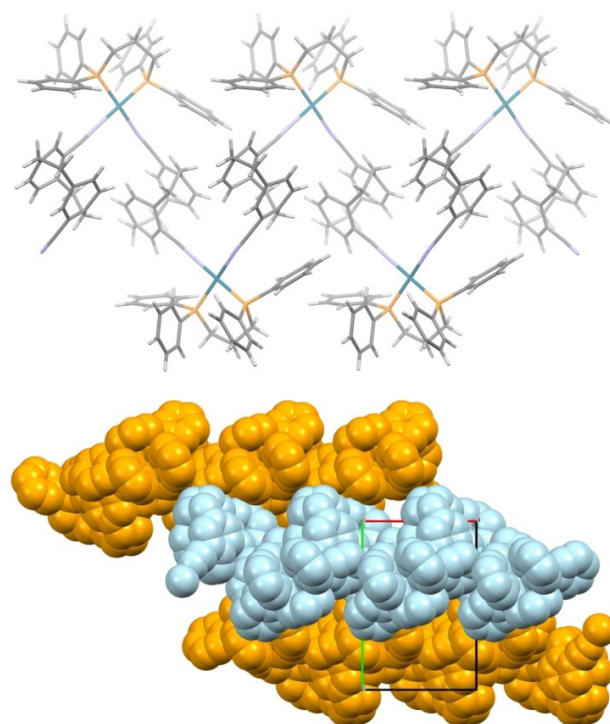

Figure 10. Top: capped sticks representation showing the helical homochiral coordination polymer $[(dppp)Pd\{(R_p)\text{-}L^{nit}\}]_n(OTf)_{2n}$ (view along the *a* axis, anions and solvent molecules are omitted for clarity, color scheme: grey–carbon, blue–nitrogen, petrol–palladium, orange–phosphorous, white–hydrogen). Bottom: space-filling representation of the coordination polymer $[(dppp)Pd\{(R_p)\text{-}L^{nit}\}]_n(OTf)_{2n}$ showing the parallel packing of the individual polymer strands (hydrogen atoms, solvent molecules and counterions are omitted for clarity).

(Figure 10). The polymeric helical strands, generated from the asymmetric unit by a twofold screw axis, are parallel to the crystallographic axis *a*. The triflate anions are placed in pockets formed by the organic ligands above and below the coordination plane of the palladium in apical positions (see Supporting Information). The complete helices are arranged in a parallel and slightly tilted brick-like packing.

A structural rearrangement also occurred when cyclopentane was diffused into a solution of heterochiral $[(dppp)_2Pd_2\{(S_p)\text{-}L^{nit}\}\{(R_p)\text{-}L^{nit}\}](OTf)_4$ in dichloromethane and the solvents were allowed to slowly evaporate. Here, however, we observed the formation of a heterochiral coordination polymer $[(dppp)_2Pd_2\{(S_p)\text{-}L^{nit}\}\{(R_p)\text{-}L^{nit}\}]_n(OTf)_{4n}$ crystallizing in the orthorhombic space group *Fdd*2. The asymmetric unit contains one ligand L^{nit}, a dppp-protected palladium ion and two disordered triflate anions. Each metal center is coordinated with one ligand of each enantiomer forming a nested-V-like structure (Figure 11). The triflate anions are located between two dppp ligands, again positioned above and below the coordination plane of the palladium centers in apical positions (see Supporting Information). The individual polymer strands are stacked in an interlocked fashion, following the [011] and [01$\bar{1}$] directions in the crystal.

Diffusion of benzene into a solution of $[(dppp)_3Pd_3\{(S_p)\text{-}L^{iso}\}_3](OTf)_6$ in acetonitrile and slow evaporation of the solvent also resulted in the formation of a homochiral coordination
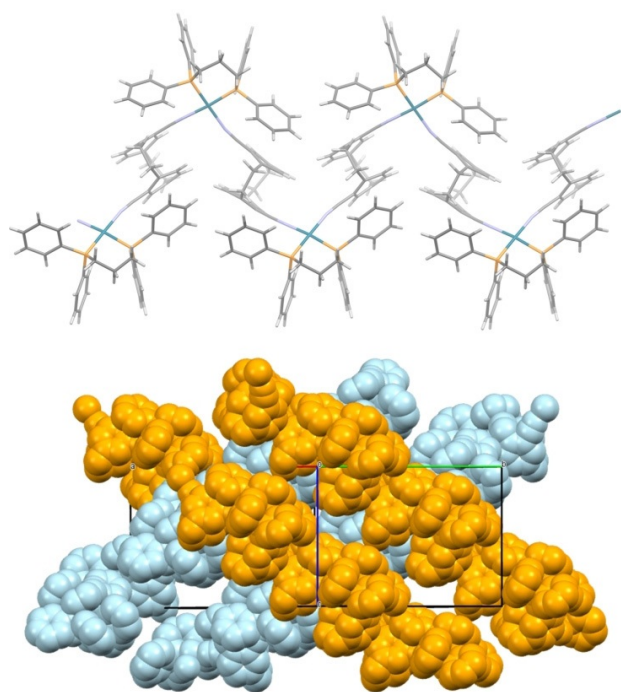
Figure 11. Top: capped sticks representation of the crystal structure of the heterochiral polymer [(dppp)$_2$Pd$_2${(S_p)-**L**^{nit}}{(R_p)-**L**^{nit}}]$_n$(OTf)$_{4n}$ showing the zig-zag-structure (view along the [011] direction, anions and solvent molecules are omitted for clarity, color scheme: grey–carbon, blue–nitrogen, petrol–palladium, orange–phosphorous, white–hydrogen); bottom: Bottom: space-filling representation of the coordination polymer [(dppp)$_2$Pd$_2${(S_p)-**L**^{nit}}{(R_p)-**L**^{nit}}]$_n$(OTf)$_{4n}$ showing the interlocked packing pattern of the individual polymer chains (hydrogen atoms, solvent molecules and counterions are omitted for clarity).

polymer [(dppp)Pd{(S_p)-**L**^{iso}}]$_n$(OTf)$_{2n}$ that turned out to be nearly isostructural to the corresponding homochiral [(dppp)Pd{(R_p)-**L**^{nit}}]$_n$(OTf)$_{2n}$ coordination polymer. The most significant difference is that solvate acetonitrile, instead of dichloromethane, is packed aligned along [100] with head-to-tail configuration between two parallel polymer chains (see Supporting Information).

Despite of our best efforts we did not succeed in obtaining crystals suitable for single-crystal XRD from solutions of the mixture of the four stereoisomers of the trinuclear complex formed from (*rac*)-**L**^{iso}.

Although the formation of helical polymeric structures from discrete cyclic structures, as observed in case of [(dppp)Pd{(S_p)-**L**^{iso}}]$_n$(OTf)$_{2n}$ and [(dppp)Pd{(R_p)-**L**^{nit}}]$_n$(OTf)$_{2n}$, is in accordance with earlier observations[10d,f,k, 11b,c, 9, 16f] and other self-assembled polymers,[6d, 9b, 37] the formation of bowl-shaped, concave, yet polymeric, structures as observed in [(dppp)$_2$Pd$_2${(S_p)-**L**^{nit}}{(R_p)-**L**^{nit}}]$_n$(OTf)$_{4n}$, is more scarce, both on the level of discrete supramolecular structures as well as on the level of self-assembled polymers.

Conclusions

We have synthesized two ligands, **L**^{nit} and **L**^{iso}, with nitrile and isonitrile metal-binding motifs, respectively, in racemic and enantiomerically pure form and investigated their coordination

behavior towards *cis*-protected palladium complex [(dppp)Pd(OTf)$_2$]. Both ligands are almost isostructural concerning the orientation of the nitrile and isonitrile groups (deviation of 1.87°), size and chirality. The only significant difference between the two constitutional isomers is in the bond strength towards the metal ion as isonitrile ligands generally coordinate much more strongly than their nitrile analogues due to better σ-donation and the superior π backbonding ability.

We studied the self-assembly and self-sorting by means of NMR spectroscopy, mass spectrometry and single-crystal X-ray diffraction studies. The aggregates of both ligands are formed selectively with regard to their composition, yielding dinuclear rhombs in case of ligand **L**^{nit} and trinuclear triangles in case of ligand **L**^{iso}. Interestingly, this difference also leads to a divergence in terms of their chiral self-sorting behavior. Ligand (*rac*)-**L**^{nit} exclusively forms achiral heterochiral dinuclear rhombs [(dppp)$_2$Pd$_2${(S_p)-**L**^{nit}}{(R_p)-**L**^{nit}}](OTf)$_4$ in a diastereoselective manner resulting from social self-sorting in non-competitive solvents like nitromethane, dichloromethane or chloroform. In contrast to this, ligand (*rac*)-**L**^{iso} rather shows a twofold preference for narcissistic self-sorting to yield a 1:1.5 mixture of racemic homo- and heterochiral trinuclear complexes. This might be due to the difference between (M-)N-C-C and (M-)C-N-C bond angles in nitrile and isonitrile complexes, respectively, being linear in the case of nitriles, with significant deviation from linearity in the case of the isonitrile groups. Obviously, it is a combination of relative binding strength between the ligands and the metal ions and the interaction with solvent molecules that is responsible for this behavior. Unfortunately, however, simulating this by state-of-the-art quantum chemical calculations is currently not possible. Thus, future studies with other ligands of similar rigidity are needed to establish whether this is a general trend. Single-crystal X-ray diffraction revealed that, upon crystallization, the discrete homo- and heterochiral aggregates rearrange to form coordination polymers.

These studies show that the self-sorting behavior is obviously not only dependent on rigid scaffolds with steric crowding or certain bend angles of V-shaped ligands, but even more on the interplay of other important factors, for example, the binding strength and mode towards the coordinated metal centers as well as the resulting structural changes in the metal binding motif.

Experimental Section

General: All solvents were distilled, dried and stored according to literature procedures. Air- and moisture-sensitive reactions were performed under argon using Schlenk techniques and oven-dried glassware. Thin layer chromatography was performed on aluminum TLC (silica 60F$_{254}$ from Merck) and detected with UV light ($\lambda =$ 254 and 366 nm). Products were purified by column chromatography on silica gel 60 (70–230 mesh) from Merck. NMR spectra were recorded at 298 K with Bruker Avance 400 or 500 spectrometer. ^{1}H and ^{13}C chemical shifts are reported on δ scale (ppm) relative to residual solvent signals (^{1}H) or the solvent signal (^{13}C) as internal standards. ^{31}P and ^{19}F chemical shifts are reported on the δ scale (ppm) relative to the chemical shifts of external standard (D$_3$PO$_4$

and TFA-*d*) measured simultaneously in a sample tube with an inset for the standard. All ^{1}H and ^{13}C signals were assigned on the basis of ^{1}H, ^{13}C, HMQC and HMBC experiments. Mass spectra were recorded with a microOTOF-Q instrument from Bruker and a MAT 90 from Thermo Finnigan. Elemental analyses were performed with a Heraeus Vario EL analyzer. However, CHN analyses could only be conducted with fluorine-free compounds. (*rac*)-4,15-diiodo[2.2]paracyclophane,[20] (*rac*)-4,15-diamino-[2.2]paracyclophane and the enantiomerically pure diamines[20] and [(dppp)Pd(OTf)$_2$][23] were prepared according to literature procedures. Numbering schemes for all compounds are included in the Supporting Information.

Synthesis of (*rac*)-, (*S*$_p$)-, (*R*$_p$)-4,15-dicyano[2.2]paracyclophane (L^{nit}): (*rac*)- or (*S*$_p$)- or (*R*$_p$)-4,15-diiodo[2.2]paracyclophane (200 mg, 0.43 mmol), zinc cyanide (408 mg, 3.48 mmol) and Pd(PPh$_3$)$_4$ (50 mg, 0.04 mmol) was dissolved in 3 mL of dry DMF and heated for 48 h at 100 °C. After cooling to room temperature, dichloromethane (10 mL) and aqueous saturated EDTA solution (5 mL) were added. The phases were separated and the aqueous layer was extracted with dichloromethane (3×20 mL). The combined organic layers were dried with MgSO$_4$, and the solvent was removed under reduced pressure. The crude product was purified by column chromatography on silica gel [eluent: cyclohexane/ethyl acetate (3:1)] to give the product ($R_f = 0.5$) as an off-white crystalline powder in 85% yield (94 mg). The analytical data are in accordance with the published ones.[19] Specific optical rotation: (−)-(*R*$_p$)-**L1**: $[\alpha]_D^{20} = -286.2 \deg \mathrm{mL} \, \mathrm{dm}^{-1} \, \mathrm{g}^{-1}$ ($c = 4.23 \, \mathrm{g} \, \mathrm{L}^{-1}$, THF), (+)-(*S*$_p$)-**L1**: $[\alpha]_D^{20} = +290.6 \deg \mathrm{mL} \, \mathrm{dm}^{-1} \, \mathrm{g}^{-1}$ ($c = 4.25 \, \mathrm{g} \, \mathrm{L}^{-1}$, THF).

Synthesis of (*rac*)-, (*S*$_p$)- or (*R*$_p$)-4,15-diformamido[2.2]*para*-cyclophane (5): (*rac*)- or (*S*$_p$)- or (*R*$_p$)-4,15-diamino[2.2]paracyclophane (34 mg, 0.14 mmol) was dissolved in 2 mL of formic acid. The solution was sonicated for 6 h. After the reaction was completed, the solution was neutralized with 6 M aqueous NaOH, diluted with 10 mL water and extracted with ethyl acetate (3×30 mL). The combined organic layers were dried with MgSO$_4$, and the solvent was removed under reduced pressure. The crude product was purified by column chromatography on silica gel [eluent: ethyl acetate] to give the product ($R_f = 0.8$) as a light brown powder in 99% yield (41 mg). ^{1}H NMR (500 MHz, [D$_6$]DMSO, 363 K > coalescence temperature): $\delta = 9.24$ (br s, 2H, H-19), 8.33 (br s, 2H, NH-17), 6.90 (br s, 2H, H-8, H-13), 6.72 (d, 2H, $^3J_{7,8} = ^3J_{12,13} = 7.6$ Hz, H-7, H-12), 6.33 (br s, 2H, H-5, H-16), 3.31–3.20 (m, 2H, H-1, H-2), 2.98–2.87 (m, 4H, H-9, H-10), 2.81–2.71 ppm (m, 2H, H-1, H-2). ^{13}C NMR (75 MHz, [D$_6$]DMSO, 298 K): $\delta = 163.9$ (C-18t), 159.0 (C-18 m), 158.9 (C-18c), 140.7 (C-4, C-15), 140.6 (C-4, C-15), 139.9 (C-4, C-15), 139.8 (C-4, C-15), 137.1 (C-6, C-11), 137.1 (C-6, C-11), 137.0 (C-6, C-11), 137.0 (C-6, C-11), 130.9 (C-8, C13), 130.8 (C-8, C13), 130.5 (C-8, C13), 130.1 (C-8, C13), 129.9 (C-3, C-14), 129.8 (C-3, C-14), 129.7 (C-3, C-14), 129.6 (C-3, C-14), 128.7 (C-7, C-12), 128.4 (C-7, C-12), 128.0 (C-7, C-12), 127.8 (C-7, C-12), 125.6 (C-5, C-16), 125.6 (C-5, C-16), 122.8 (C-5, C-16), 122.8 (C-5, C-16), 34.2 (C-9, C-10), 34.1 (C-9, C-10), 34.0 (C-9, C-10), 30.7 (C-1, C-2), 30.5 (C-1, C-2), 30.3 (C-1, C-2), 30.2 (C-1, C-2), 30.1 ppm (C-1, C-2). MS (EI) *m/z* (intensity %) = 294.1 (95) $[M]^{+\bullet}$, 266.1 (25) $[M-\mathrm{CO}]^+$, 147.1 (70) $[M-\mathrm{C_9H_9NO}]^+$, 132.1 (5) $[M-\mathrm{C_{10}H_{12}NO}]^+$, 119.1 (100) $[M-\mathrm{C_{10}H_9NO_2}]^+$, 104.1 (35) $[M-\mathrm{C_{11}H_{12}NO_2}]^+$. High resolution MS (EI): *m/z* = 294.1368 (calcd for $[\mathrm{C_{18}H_{18}N_2O_2}]^{+\bullet}$ 294.1368).

Synthesis of (*rac*)-, (*S*$_p$)-, (*R*$_p$)-4,15-diisocyano[2.2]paracyclophane (L^{iso}): (*rac*)- or (*S*$_p$)- or (*R*$_p$)-**5** (70 mg, 0.24 mmol) was suspended in an equal mixture of THF and triethylamine (8 mL). Addition of 0.5 mL (5.52 mmol, 23 equiv) POCl$_3$ turned the suspension in a reddish solution which was stirred for 13 h and quenched with aqueous saturated NaCl (3 mL) and 2 M NaOH (10 mL) under cooling.

The aqueous phase was extracted with ethyl acetate (3×20 mL). The combined organic layers were dried with MgSO$_4$, and the solvent was removed under reduced pressure. The crude product was purified by column chromatography on silica gel [eluent: cyclohexane/ethyl acetate (5:1)] to give the product ($R_f = 0.5$) as a light yellow crystalline solid in 73% yield (45 mg). ^{1}H NMR (400 MHz, CDCl$_3$, 298 K): $\delta = 7.17$ (d, 2H, $^3J_{8,7} = ^3J_{13,12} = 8.0$ Hz, H-8, H-13), 6.61 (dd, 2H, $^3J_{7,8} = ^3J_{12,13} = 8.0$ Hz, $^4J_{7,5} = ^4J_{12,16} = 1.9$ Hz, H-7, H-12), 6.41 (d, 2H, $^4J_{5,7} = ^4J_{16,12} = 1.9$ Hz, H-5, H-16), 3.49–3.38 (m, 2H, H-9, H-10), 3.19–2.97 ppm (m, 6H, H-9, H-10, H-1, H-2). ^{13}C NMR (101 MHz, CDCl$_3$, 298 K): $\delta = 166.1$ (C-17), 141.4 (C-3, C-14), 136.7 (C-6, C-11), 133.1 (C-7, C-12), 131.7 (C-5, C-16), 130.2 (C-8, C-13), 128.8 (C-17), 34.5 (C-1, C-2), 30.4 ppm (C-9, C-10). MS (EI) *m/z* (intensity %) = 258.2 (10) $[M]^{+\bullet}$, 129.1 (10) $[M-\mathrm{C_9H_7N}]^+$, 101.2 (20) $[M-\mathrm{C_2H_4}]^+$. High resolution MS(EI): *m/z* = 257.1076 (calcd for $[\mathrm{C_{18}H_{14}N_2}-\mathrm{H}]^+$: 257.1079). $\mathrm{C_{18}H_{14}N_2}\cdot\frac{1}{6}$ (258.32 g mol^{-1}): calcd C 80.08.18, H 5.30, N 10.28; found C 80.05, H 5.62, N 9.87. Specific optical rotation: (+)-(*S*$_p$)-**L2**: $[\alpha]_D^{20} = +284.1 \deg \mathrm{mL} \, \mathrm{dm}^{-1} \, \mathrm{g}^{-1}$ ($c = 2.37 \, \mathrm{g} \, \mathrm{L}^{-1}$, CHCl$_3$), (−)-(*R*$_p$)-**L2**: $-287.4 \, \mathrm{mL} \, \mathrm{dm}^{-1} \, \mathrm{g}^{-1}$ ($c = 2.42 \, \mathrm{g} \, \mathrm{L}^{-1}$, CHCl$_3$).

Synthesis of [(dppp)$_2$Pd$_2${(*S*$_p$)-L^{nit}}{(*R*$_p$)-L^{nit}}](OTf)$_4$, [(dppp)$_2$Pd$_2${(*R*$_p$)-L^{nit}}$_2$](OTf)$_4$ and [(dppp)$_2$Pd$_2${(*S*$_p$)-L^{nit}}$_2$](OTf)$_4$: (*rac*)-, (*S*$_p$)-, or (*R*$_p$)-**L1** (5 mg, 19.4 µmol) was dissolved in 0.4 mL CD$_3$NO$_2$. To this, a solution of [(dppp)Pd(OTf)$_2$] (15.8 mg, 19.4 µmol) in 0.4 mL CD$_3$NO$_2$ was added. The solution turned pale yellow indicating the formation of the complex. The solution was characterized by NMR spectroscopy.
Analytical data of [(dppp)$_2$Pd$_2${(*R*$_p$)-L^{nit}}$_2$]OTf$_4$ and its enantiomer obtained from optically pure ligands (*R*$_p$)-L^{nit} and (*S*$_p$)-L^{nit}, respectively: ^{1}H NMR (499 MHz, CD$_3$NO$_2$, 298 K): $\delta = 7.89$–7.79 (m, 16H, H$_{dppp(phenyl)}$), 7.71–7.64 (m, 8H, H$_{dppp(phenyl)}$), 7.61–7.54 (m, 16H, H$_{dppp(phenyl)}$), 6.85–6.78 (m, 8H, H-8, H-13, H-5, H-16, H-7, H-12), 3.28–3.06 (m, 16H, H-1, H-2, H-9, H-10), 2.97–2.89 (m, 8H, PCH$_2$CH$_2$CH$_2$P), 2.53–2.37 ppm (m, 4H, PCH$_2$CH$_2$CH$_2$P). DOSY: $D = 5.42 \times 10^{-6} \, \mathrm{cm^2 \, s^{-1}}$. ^{31}P NMR (202 MHz, CD$_3$NO$_2$, 298 K): $\delta = 17.18$ ppm (s). ^{19}F-NMR (470 MHz, CD$_3$NO$_2$, 298 K): $\delta = -79.26$ ppm (s).

Analytical data for [(dppp)$_2$Pd$_2${(*S*$_p$)-L^{nit}}{(*R*$_p$)-L^{nit}}](OTf)$_4$ obtained from (*rac*)-L^{nit}: ^{1}H NMR (499 MHz, CD$_3$NO$_2$, 298 K): $\delta = 7.86$–7.78 (m, 16H, H$_{dppp(phenyl)}$), 7.70–7.64 (m, 8H, H$_{dppp(phenyl)}$), 7.60–7.54 (m, 16H, H$_{dppp(phenyl)}$), 6.84–6.75 (m, 8H, H-8, H-13, H-5, H-16, H-7, H-12), 3.25–3.04 (m, 16H, H-1, H-2, H-9, H-10), 2.96–2.89 (m, 8H, PCH$_2$CH$_2$CH$_2$P), 2.52–2.36 ppm (m, 4H, PCH$_2$CH$_2$CH$_2$P). DOSY: $D = 5.26 \times 10^{-6} \, \mathrm{cm^2 \, s^{-1}}$. ^{31}P NMR (202 MHz, CD$_3$NO$_2$, 298 K): $\delta = 17.80$ ppm (s). ^{19}F NMR (470 MHz, CD$_3$NO$_2$, 298 K): $\delta = -79.24$ ppm (s).

Synthesis of [(dppp)$_2$Pd$_2${(*S*$_p$)-L^{iso}}$_2${(*R*$_p$)-L^{iso}}](OTf)$_4$/ [(dppp)$_2$Pd$_2${(*R*$_p$)-L^{iso}}$_2${(*S*$_p$)-L^{iso}}](OTf)$_4$, [(dppp)$_3$Pd$_3${(*S*$_p$)-L^{iso}}$_3$](OTf)$_6$, and [(dppp)$_3$Pd$_3${(*R*$_p$)-L^{iso}}$_3$](OTf)$_6$: (*rac*)-, (*S*$_p$)-, or (*R*$_p$)-L^{iso} (5 mg, 19.4 µmol) was dissolved in 0.4 mL CD$_3$NO$_2$. To this, a solution of [(dppp)Pd(OTf)$_2$] (15.8 mg, 19.4 µmol) in 0.4 mL CD$_3$NO$_2$ was added. The solution turned pale yellow indicating the formation of the complex. The solution was characterized by NMR spectroscopy and ESI-MS.

Analytical data for [(dppp)$_3$Pd$_3${(*R*$_p$)-L^{iso}}$_3$](OTf)$_6$ and its enantiomer obtained from (*R*$_p$)-L^{iso} and (*R*$_p$)-L^{iso}, respectively: ^{1}H NMR (499 MHz, CD$_3$NO$_2$, 298 K): $\delta = 7.88$–7.79 (m, 12H, H$_{dppp(phenyl)}$), 7.79–7.66 (m, 18H, H$_{dppp(phenyl)}$), 7.66–7.54 (m, 18H, H$_{dppp(phenyl)}$), 7.54–7.44 (m, 12H, H$_{dppp(phenyl)}$), 6.60 (d, 6H, $^3J_{8,7} = ^3J_{13,12} = 8.6$ Hz, H-8, H-13), 6.45 (d, 6H, $^3J_{7,8} = ^3J_{12,13} = 8.6$ Hz, $^4J_{7,5} = ^4J_{12,16} = 1.8$ Hz, H-7, H-12), 5.80 (d, 6H, $^4J_{5,7} = ^4J_{16,12} = 1.8$ Hz, H-5, H-16), 3.30–3.21 (m, 6H, H-1, H-2, H-9, H-10), 3.09–2.88 (m, 30H, H-1, H-2, H-9, H-10, PCH$_2$CH$_2$CH$_2$P), 2.58–2.40 ppm (m, 6H, PCH$_2$CH$_2$CH$_2$P). DOSY: $D = 3.12 \times 10^{-6} \, \mathrm{cm^2 \, s^{-1}}$. ^{31}P NMR (202 MHz, CD$_3$NO$_2$, 298 K): $\delta = 1.91$ ppm (s). ^{19}F NMR (470 MHz, CD$_3$NO$_2$, 298 K): $\delta = -79.06$ ppm (s). MS-ESI (positive, 8 eV) *m/z* = 555.0 $[\mathrm{Pd(dppp)Cl}]^+$, 667.0 $[\mathrm{Pd(dppp)(OTf)}]^+$, 683.1 $[\mathrm{Pd_2(dppp)_2Cl_2}]^+$, 811.2 $[\mathrm{Pd(dppp)Cl}]^+$, 926.1

$[Pd_3(dppp)_3(\mathbf{L^{iso}})_3(OTf)_3]^{3+}$ and $[Pd(dppp)(\mathbf{L^{iso}})(OTf)]^+$, 1463.7 $[Pd_3(dppp)_3(\mathbf{L^{iso}})_3(OTf)_3]^{2+}$.

Analytical data for the mixture of complexes obtained from (rac)-$\mathbf{L^{iso}}$: ^1H NMR (499 MHz, CD_3NO_2, 298 K, ratio homochiral: heterochiral 1:1.5): $\delta = 8.03-7.26$ (m, $H_{dppp(phenyl)}$ (homo- and heterochiral)), 6.96 (d, 2H, $^3J_{8,7} = ^3J_{13,12} = 8.1$ Hz, H-8/H-13 (heterochiral)), 6.74 (dd, 2H, $^3J_{7,8} = ^3J_{12,13} = 8.1$ Hz, $^4J_{7,5} = ^4J_{12,16} = 1.7$ Hz, H-7/H-12 (heterochiral)), 6.60 (d, 2H, $^3J_{8,7} = ^3J_{13,12} = 8.1$ Hz, H-8/H-13 (homochiral)), 6.48–6.42 (m, H-7/H-12 (homochiral), H-7'/H-12' (heterochiral), H-8'/H-13' (heterochiral)), 6.37 (d, 2H, $^3J_{8,7} = ^3J_{13,12} = 8.1$ Hz, H-8''/H-13'' (heterochiral), 6.31 (d, 2H, $^4J_{5,7} = ^4J_{16,12} = 1.8$ Hz, H-5/H-16 (heterochiral)), 6.26 (dd, 2H, $^3J_{7,8} = ^3J_{12,13} = 8.1$ Hz, $^4J_{7,5} = ^3J_{12,16} = 1.7$ Hz, H-7''/H-12''(heterochiral)), 5.93 (d, 2H, $^4J_{5,7} = ^4J_{16,12} = 1.8$ Hz, H-5'/H-16' (heterochiral)), 5.80 (d, 2H, $^4J_{5,7} = ^4J_{16,12} = 1.8$ Hz, H-5/H-16 (homochiral)), 5.61 (d, 2H, $^4J_{5,7} = ^4J_{16,12} = 1.8$ Hz, H-5''/H-16'' (heterochiral)), 3.32–3.29 (m, $H_{ethylbridges}$, $PCH_2CH_2CH_2P$ (homo- and heterochiral)), 2.60–2.39 ppm (m, $PCH_2CH_2CH_2P$ (homo- and heterochiral)). DOSY: $D = 3.20 \times 10^{-6}$ cm^{2}s^{-1}. ^{31}P NMR (202 MHz, CD_3NO_2, 298 K, ratio homochiral : heterochiral 1:1.5): $\delta = 2.12$ (s (heterochiral)), 1.95 (d, $^2J_{PP} = 18.1$ Hz (heterochiral)), 1.94 (s (homochiral)), 1.69 ppm (d, $^2J_{PP} = 18.1$ Hz (heterochiral)). ^{19}F NMR (470 MHz, CD_3NO_2, 298 K): $\delta = -79.03$ ppm (s). MS-ESI (positive, 8 eV) $m/z = 555.0$ $[Pd(dppp)Cl]^+$, 667.0 $[Pd(dppp)(OTf)]^+$, 683.1 $[Pd_2(dppp)_2Cl_2]^+$, 811.2 $[Pd(dppp)Cl]^+$, 926.1 $[Pd_3(dppp)_3(\mathbf{L^{iso}})_3(OTf)_3]^{3+}$ and $[Pd(dppp)(\mathbf{L^{iso}})(OTf)]^+$, 1463.7 $[Pd_3(dppp)_3(\mathbf{L^{iso}})_3(OTf)_3]^{2+}$.

Computational details

All spectra calculations were performed for the R_p-enantiomer.

Two approaches were pursued for the calculation of the UV/Vis and ECD spectra of $\mathbf{L^{nit}}$. First, a single structure of $\mathbf{L^{nit}}$ was prepared and optimized using the composite method PBEh-3c and the implicit solvation model COSMO($\varepsilon = 36.6$). On the optimized geometry a sTD-CAM-B3LYP/def2-TZVP[38] calculation including proceeding ground state calculation was performed using sTD-DFT[21] as implemented in ORCA 4.0.1.[39] The length form of the electric dipole transition moment is employed for the absorption spectra whereas the velocity form is used for the ECD spectra, which is guaranteeing gauge origin independence. The computed spectra (UV/Vis and ECD) are redshifted by 0.2 eV to roughly match the experimental spectrum. In the second approach, conformational flexibility is considered for the spectrum by generating snapshots from a GFN1-xTB/GBSA(acetonitrile)[40] molecular dynamics simulation (at 298 K, using $H_{mass} = 4$ amu, time step(dt fs^{-1}) = 1.0, md time = 1000 ps, and using the SHAKE algorithm). From the molecular dynamic simulation the equilibration phase was removed and 200 equidistant snapshots were obtained. On these, sTD-BH-LYP/def2-SVP/COSMO($\varepsilon = 36.6$)[41] calculations were performed using the Turbomole 7.0.2 program package[42] and the sTDA standalone program.[43] The computed spectra (UV/Vis and ECD) are redshifted by 0.4 eV to roughly match the experimental spectrum. Free energies as discussed in the main text were calculated by using the following protocol: all geometries were prepared manually and pre-optimized with the semiempirical quantum chemical method GFN2-xTB/GBSA(CH$_3$CN).[34] The geometries were subsequently optimized with the composite method PBEh-3c[33] and the implicit solvation model DCOSMO-RS(NO$_2$CH$_3$) by using the Turbomole program package. On the optimized geometries free energies are calculated using a multilevel approach.[44] High level single-point energies were calculated with the hybrid density functional PBE0[29] in a large def2-QZVP[30] basis set. The (long-range) London dispersion not accounted for by the density functional was computed with the DFT-D4[31] method at default settings. Solvation contributions

to free energy were calculated with COSMO-RS.[32] This term includes the volume work $RT\ln(V_{ideal})$ to go from an ideal gas at 1 bar to 1 mol L^{-1}. Thermostatistical contributions to free energy were calculated using GFN2-xTB/GBSA(CH$_3$CN) and the slightly modified RRHO-Scheme (interpolation between the rigid-rotor- to the harmonic-oscillator is applied at low-lying frequencies, see Ref. [44]). The total free energies are then calculated as the sum of the single-point energy, dispersion contribution, thermostatistical and solvation contribution. The B3LYP/QZ-SMD[45] single-point calculations were performed with the ORCA 4.1.0 with convergence criteria for single point energies: 1.0×10^{-6} E_h. All DFT (except for the B3LYP[46] single-point) calculations were performed by using the TURBOMOLE 7.2.1 program package. The resolution-of-identity (RI) approximation for the Coulomb integrals[47] was generally applied using the matching default auxiliary basis sets.[48] The integration of the exchange-correlation contribution was evaluated on the numerical quadrature grids m4 for PBEh-3c and PBE0. The default convergence criteria for single-point energies were 10^{-7} E_h. For the conductor-like screening model for real solvents (COSMO-RS) free energy, two single-point calculations with BP86/TZ (one in gas-phase and one in an ideal conductor) have to be performed. The output of these calculations is then processed by the COSMOtherm program.[49]

Crystallographic details

Data for (S_p)-$\mathbf{L^{nit}}$, (S_p)-$\mathbf{L^{iso}}$ and $[(dppp)Pd\{(R_p)\text{-}\mathbf{L^{nit}}\}]_n(OTf)_{2n}$ were collected on a Bruker D8 Venture diffractometer, equipped with a low temperature device (Cryostream 800er series, Oxford Cryosystems, Oxford) using mirror-monochromated Cu Kα radiation ($\lambda = 1.54184$ Å) of Mo Kα radiation ($\lambda = 0.71073$ Å). Intensities were measured by fine-slicing ϕ- and ω-scans and corrected for background, polarization and Lorentz effects. Semiempirical absorption corrections were applied for all data sets following Blessing's method.[50] The structures were solved by intrinsic phasing methods[51] and refined anisotropically by the least-squares procedure implemented in the ShelX program system.[52] The hydrogen atoms were included isotropically by using the riding model on the bound carbon atoms.

Data for $[(dppp)_2Pd_2\{(S_p)\text{-}\mathbf{L^{nit}}\}\{(R_p)\text{-}\mathbf{L^{nit}}\}]_n(OTf)_{4n}$ and $[(dppp)Pd\{(S_p)\text{-}\mathbf{L^{iso}}\}]_n(OTf)_{2n}$ were collected on an Agilent SuperNova Dual diffractometer, equipped with a low-temperature device (Cryostream 700, Oxford Cryosystems, Oxford) using mirror-monochromated Cu Kα radiation ($\lambda = 1.54184$ Å). CrysAlisPro[51] software was used for data collection and reduction as well as applying numerical absorption correction based on gaussian integration. The structure was solved by a dual-space algorithm using SHELXT-2014/5[52] and refined by full-matrix least squares on F^2 using SHELXL-2017/1[53] within Olex2[54] and WinGX[55] environments. All non-hydrogen atoms were refined anisotropically. All carbon-bound hydrogen atoms were calculated to their optimal positions and treated as riding on the parent atoms using isotropic displacement parameters 1.2 (or 1.5 in case of methyl groups) times larger than the respective parent atoms. Appropriate geometry restraints were applied to the anions, making the 1,2- and 1,3-distances equal. Rigid bond restraints were applied to the atomic displacement parameters of the anions and solvents. Triflate anions in $[(dppp)_2Pd_2\{(S_p)\text{-}\mathbf{L^{nit}}\}\{(R_p)\text{-}\mathbf{L^{nit}}\}]_n(OTf)_{4n}$ were found to exhibit both substitutional and positional disorder, and were modelled accordingly, with their relative occupancies freely refined and the similarity restraints applied to their atomic displacement parameters.

Crystallographic data and refinement parameters are shown in Table 3. CCDC 1824416 $([(dppp)_2Pd_2\{(S_p)\text{-}\mathbf{L^{nit}}\}\{(R_p)\text{-}\mathbf{L^{nit}}\}]_n(OTf)_{4n})$, 1824417 $([(dppp)Pd\{(S_p)\text{-}\mathbf{L^{iso}}\}]_n(OTf)_{2n})$, 1955599 $((S_p)\text{-}\mathbf{L^{nit}})$, 1955600

Table 3. Crystallographic data for (S_p)-$\mathbf{L^{nit}}$, (S_p)-$\mathbf{L^{iso}}$, $[(\text{dppp})\text{Pd}\{(R_p)\text{-}\mathbf{L^{nit}}\}]_n(\text{OTf})_{2n}$, $[(\text{dppp})_2\text{Pd}_2\{(S_p)\text{-}\mathbf{L^{nit}}\}\{(R_p)\text{-}\mathbf{L^{nit}}\}]_n(\text{OTf})_{4n}$ and $[(\text{dppp})\text{Pd}\{(S_p)\text{-}\mathbf{L^{iso}}\}]_n(\text{OTf})_{2n}$.

Compound		(S_p)-$\mathbf{L^{nit}}$	(R_p)-$\mathbf{L^{iso}}$	$[(\text{dppp})_2\text{Pd}_2\{(Sp)\text{-}\mathbf{L^{nit}}\}\{(R_p)\text{-}\mathbf{L^{nit}}\}]_n(\text{OTf})_{4n}$	$[(\text{dppp})\text{Pd}\{(R_p)\text{-}\mathbf{L^{nit}}\}]_n(\text{OTf})_{2n}$	$[(\text{dppp})\text{Pd}\{(S_p)\text{-}\mathbf{L^{iso}}\}]_n(\text{OTf})_{2n}$
CCDC number		1955599	1955600	1824416	1955601	1824417
empirical formula		$C_{18}H_{14}N_2$	$C_{18}H_{14}N_2$	$[C_{45}H_{40}N_2P_2Pd]^{2+}\ 2(CF_3SO_3)^-$	$[C_{48}H_{42}Cl_2F_6N_2O_6P_2PdS_2]$	$[C_{45}H_{40}N_2P_2Pd]^{2+}$ $2(CF_3SO_3)^-\ C_2H_3N$
M [g mol^{-1}]		258.31	258.31	1075.27	1160.19	1116.32
T [K]		100	100	123.0(1)	100	123.0(1)
radiation type		Cu Kα	Cu Kα	Cu Kα	Mo Kα	Cu Kα
λ [Å]		1.54178	1.54178	1.54184	0.71073	1.54184
crystal system		orthorhombic	orthorhombic	orthorhombic	orthorhombic	orthorhombic
space group		$P2_12_12_1$	$P2_12_12_1$	$Fdd2$	$P2_12_12_1$	$P2_12_12_1$
unit cell	a [Å]	7.3642(5)	7.3476(4)	51.7823(8)	10.9490(14)	11.0937(2)
parameters	b [Å]	12.3891(10)	12.5435(8)	23.0531(3)	16.206(2)	16.2458(3)
	c [Å]	14.3728(11)	14.3903(9)	15.9229(3)	27.128(3)	26.8214(6)
	α [°]	90	90	90	90	90
	β [°]	90	90	90	90	90
	γ [°]	90	90	90	90	90
$V_{\text{unit cell}}$ [Å^3]		1311.31(17)	1326.28(14)	19007.8(5)	4813.6(10)	4833.91(17)
Z		4	4	16	4	4
ρ_{calcd} [g cm^{-3}]		1.308	1.294	1.503	1.601	1.534
absorption correction		multi-scan	multi-scan	Gaussian	multi-scan	Gaussian
absorption coefficient μ [mm^{-1}]		0.602	0.595	5.258	0.725	5.186
min. and max. transmission		0.3762, 0.7535	0.4073, 0.7536	0.469, 0.738	0.5689, 0.7459	0.605, 0.846
$F(000)$		544.0	544.0	8736.0	2352.0	2272.0
crystal color		clear colorless	clear colorless	pale yellow	clear colorless	pale yellow
crystal size [mm^3]		$0.30\times0.16\times0.05$	$0.11\times0.07\times0.05$	$0.258\times0.103\times0.069$	$0.21\times0.06\times0.05$	$0.153\times0.115\times0.034$
2θ range for data coll [°]		9.424 to 135.482	9.352 to 134.958	6.828 to 149.028	4.49 to 55.998	8.550 to 148.196
reflns collected		16145	3883	73632	92605	15248
[R(int)]		[0.0542]	[0.0235]	[0.0386]	[0.1572]	[0.0401]
reflns [$I > 2\sigma(I)$]		2377	2109	9333	11632	7804
data completeness [%]		99.9	95.6	100.0	99.9	99.2
data/parameters/restraints		2377/181/0	2109/182/0	9592/741/955	11632/632/0	9334/624/214
goodness-of-fit on F^2		1.069	1.077	1.048	1.026	1.065
final R indices [$I > 2\sigma(I)$]		$R1 = 0.0372$ $wR2 = 0.0929$	$R1 = 0.0325$ $wR2 = 0.0811$	$R1 = 0.0368$ $wR2 = 0.0960$	$R1 = 0.0534$ $wR2 = 0.0995$	$R1 = 0.0538$ $wR2 = 0.1358$
final R indices [all data]		$R1 = 0.0378$ $wR2 = 0.0936$	$R1 = 0.0345$ $wR2 = 0.0824$	$R1 = 0.0387$ $wR2 = 0.1002$	$R1 = 0.1208$ $wR2 = 0.1214$	$R1 = 0.0678$ $wR2 = 0.1459$
largest diff. peak/ hole [e Å^{-3}]		0.23/−0.29	0.15/−0.19	1.085/−0.583	1.56/−1.57	1.843/−0.671
Flack parameter x		0.3(2)	0.1(7)	−0.016(4)	0.004(14)	−0.036(7)
$P2$(true) value		0.990	1.000	–	1.000	–
torsion angles binding units [°]		119.81	117.94	125.57	−132.66	−129.92

$((S_p)$-$\mathbf{L^{iso}})$, and 1955601 ($[(\text{dppp})\text{Pd}\{(R_p)\text{-}\mathbf{L^{nit}}\}]_n(\text{OTf})_{2n})$ contain the supplementary crystallographic data for this paper. These data are provided free of charge by The Cambridge Crystallographic Data Centre.

Acknowledgements

Conflict of interest

The authors declare no conflict of interest.

[1] a) A. Wu, L. Isaacs, *J. Am. Chem. Soc.* **2003**, *125*, 4831–4835; b) K. Osowska, O. Miljanić, *Synlett* **2011**, 1643–1648; c) M. M. Safont-Sempere, G. Fernández, F. Würthner, *Chem. Rev.* **2011**, *111*, 5784–5814; d) M. Lal Saha, M. Schmittel, *Org. Biomol. Chem.* **2012**, *10*, 4651–4684; e) Z. He, W. Jiang, C. A. Schalley, *Chem. Soc. Rev.* **2015**, *44*, 779–789.
[2] P. N. Taylor, H. L. Anderson, *J. Am. Chem. Soc.* **1999**, *121*, 11538–11545.
[3] R. Krämer, J.-M. Lehn, A. Marquis-Rigault, *Proc. Natl. Acad. Sci. USA* **1993**, *90*, 5394–5398.
[4] A. Shivanyuk, J. Rebek, *J. Am. Chem. Soc.* **2002**, *124*, 12074–12075.
[5] T. W. Kim, J.-I. Hong, M. S. Lah, *Chem. Commun.* **2001**, 743–744.

[6] a) D. K. Smith, *Chem. Soc. Rev.* **2009**, *38*, 684–694; b) T. F. A. De Greef, M. M. J. Smulders, M. Wolffs, A. P. H. J. Schenning, R. P. Sijbesma, E. W. Meijer, *Chem. Rev.* **2009**, *109*, 5687–5754; c) K. Sato, Y. Itoh, T. Aida, *Chem. Sci.* **2014**, *5*, 136–140; d) M. Liu, L. Zhang, T. Wang, *Chem. Rev.* **2015**, *115*, 7304–7397.

[7] a) *Supramolecular Chirality* (Eds.: M. Crego-Calama, D. N. Reinhoudt) Springer, Berlin, **2006**; b) *Chirality in Supramolecular Assemblies: Causes and Consequences*, (Ed.: F. R. Keene), Wiley, Chichester, **2016**; c) H. Jędrzejewska, A. Szumna, *Chem. Rev.* **2017**, *117*, 4863–4899.

[8] Examples for social chiral self-sorting of ligands with chelating metal-binding motifs: a) M. Kitamura, S. Okada, S. Suga, R. Noyori, *J. Am. Chem. Soc.* **1989**, *111*, 4028–4036; b) H. C. Aspinall, J. F. Bickley, J. L. M. Dwyer, N. Greeves, R. V. Kelly, A. Steiner, *Organometallics* **2000**, *19*, 5416–5423; c) R. Wang, M. Hong, D. Yuan, Y. Sun, L. Xu, J. Luo, R. Cao, A. S. C. Chan, *Eur. J. Inorg. Chem.* **2004**, 37–43; d) J. M. Takacs, P. M. Hrvatin, J. M. Atkins, D. S. Reddy, J. L. Clark, *New J. Chem.* **2005**, *29*, 263–265.

[9] Examples for social chiral self-sorting of ligands with monodentate metal binding motifs: a) C. G. Claessens, T. Torres, *J. Am. Chem. Soc.* **2002**, *124*, 14522–14523; b) T. J. Burchell, R. J. Puddephatt, *Inorg. Chem.* **2005**, *44*, 3718–3730; c) M. Mizumura, H. Shinokubo, A. Osuka, *Angew. Chem. Int. Ed.* **2008**, *47*, 5378–5381; *Angew. Chem.* **2008**, *120*, 5458–5461; d) C. G. Claessens, I. Sánchez-Molina, T. Torres, *Supramol. Chem.* **2009**, *21*, 44–47; e) T. Weilandt, U. Kiehne, G. Schnakenburg, A. Lützen, *Chem. Commun.* **2009**, 2320–2322; f) T. Weilandt, U. Kiehne, J. Bunzen, G. Schnakenburg, A. Lützen, *Chem. Eur. J.* **2010**, *16*, 2418–2426; g) J. J. Henkelis, C. J. Carruthers, S. E. Chambers, R. Clowes, A. I. Cooper, J. Fisher, M. J. Hardie, *J. Am. Chem. Soc.* **2014**, *136*, 14393–14396.

[10] a) Examples for narcissistic chiral self-sorting of ligands with chelating metal binding motifs: D. L. Caulder, K. N. Raymond, *Angew. Chem. Int. Ed. Engl.* **1997**, *36*, 1440–1442; *Angew. Chem.* **1997**, *109*, 1508–1510; b) M. A. Masood, E. J. Enemark, T. D. P. Stack, *Angew. Chem. Int. Ed.* **1998**, *37*, 928–932; *Angew. Chem.* **1998**, *110*, 973–977; c) M. Albrecht, M. Schneider, H. Röttele, *Angew. Chem. Int. Ed.* **1999**, *38*, 557–559; *Angew. Chem.* **1999**, *111*, 512–515; d) J.-M. Vincent, C. Philouze, I. Pianet, J.-B. Verlhac, *Chem. Eur. J.* **2000**, *6*, 3595–3599; e) A. Lützen, M. Hapke, J. Griep-Raming, D. Haase, W. Saak, *Angew. Chem. Int. Ed.* **2002**, *41*, 2086–2089; *Angew. Chem.* **2002**, *114*, 2190–2194; f) M. Albrecht, R. Fröhlich, *Bull. Chem. Soc. Jpn.* **2007**, *80*, 797–808; g) U. Kiehne, T. Weilandt, A. Lützen, *Org. Lett.* **2007**, *9*, 1283–1286; h) P. L. Arnold, J.-C. Buffet, R. P. Blaudeck, S. Sujecki, A. J. Blake, C. Wilson, *Angew. Chem. Int. Ed.* **2008**, *47*, 6033–6036; *Angew. Chem.* **2008**, *120*, 6122–6125; i) J. Bunzen, T. Bruhn, G. Bringmann, A. Lützen, *J. Am. Chem. Soc.* **2009**, *131*, 3621–3630; j) N. Dalla Favera, U. Kiehne, J. Bunzen, S. Hytteballe, A. Lützen, C. Piguet, *Angew. Chem. Int. Ed.* **2010**, *49*, 125–128; *Angew. Chem.* **2010**, *122*, 129–132; k) C. Gütz, R. Hovorka, N. Struch, J. Bunzen, G. Meyer-Eppler, Z.-W. Qu, S. Grimme, F. Topić, K. Rissanen, M. Cetina, M. Engeser, A. Lützen, *J. Am. Chem. Soc.* **2014**, *136*, 11830–11838; l) A. Jarzebski, C. Tenten, C. Bannwarth, G. Schnakenburg, S. Grimme, A. Lützen, *Chem. Eur. J.* **2017**, *23*, 12380–12386; m) N. Struch, C. Frömbgen, G. Schnakenburg, A. Lützen, *Eur. J. Org. Chem.* **2017**, 4984–4989.

[11] a) Examples for narcissistic chiral self-sorting of ligands with monodentate metal binding motifs: L. Isaacs, D. Witt, *Angew. Chem. Int. Ed.* **2002**, *41*, 1905–1907; *Angew. Chem.* **2002**, *114*, 1985–1987; b) H.-J. Kim, D. Moon, M. S. Lah, J.-I. Hong, *Angew. Chem. Int. Ed.* **2002**, *41*, 3174–3177; *Angew. Chem.* **2002**, *114*, 3306–3309; c) I.-W. Hwang, T. Kamada, T. K. Ahn, D. M. Ko, T. Nakamura, A. Tsuda, A. Osuka, D. Kim, *J. Am. Chem. Soc.* **2004**, *126*, 16187–16198; d) T. J. Burchell, R. J. Puddephatt, *Inorg. Chem.* **2006**, *45*, 650–659; e) T. Kamada, N. Aratani, T. Ikeda, N. Shibata, Y. Higuchi, A. Wakamiya, S. Yamaguchi, K. S. Kim, Z. S. Yoon, D. Kim, A. Osuka, *J. Am. Chem. Soc.* **2006**, *128*, 7670–7678; f) C. Maeda, T. Kamada, N. Aratani, A. Osuka, *Coord. Chem. Rev.* **2007**, *251*, 2743–2752; g) T. K. Ronson, J. Fisher, L. P. Harding, M. J. Hardie, *Angew. Chem. Int. Ed.* **2007**, *46*, 9086–9088; *Angew. Chem.* **2007**, *119*, 9244–9246; h) K. Schober, H. Zhang, R. M. Gschwind, *J. Am. Chem. Soc.* **2008**, *130*, 12310–12317; i) C. Gütz, R. Hovorka, G. Schnakenburg, A. Lützen, *Chem. Eur. J.* **2013**, *19*, 10890–10894; j) C. Gütz, R. Hovorka, C. Stobe, N. Struch, F. Topić, G. Schnakenburg, K. Rissanen, A. Lützen, *Eur. J. Org. Chem.* **2014**, 206–216; k) G. Meyer-Eppler, F. Topić, G. Schnakenburg, K. Rissanen, A. Lützen, *Eur. J. Inorg. Chem.* **2014**, 2495–2501; l) R. Hovorka, S. Hytteballe, T. Piehler, G. Meyer-Eppler, F. Topić, K. Rissanen, M. Engeser, A. Lützen, *Beil-*

stein J. Org. Chem. **2014**, *10*, 432–441; m) T. Tateishi, T. Kojima, S. Hiraoka, *Commun. Chem.* **2018**, *1*, 20; n) S. Kai, T. Kojima, F. L. Thorp-Greenwood, M. J. Hardie, S. Hiraoka, *Chem. Sci.* **2018**, *9*, 4104–4108; o) J. Anhäuser, R. Puttreddy, Y. Lorenz, A. Schneider, M. Engeser, K. Rissanen, A. Lützen, *Org. Chem. Front.* **2019**, *6*, 1226–1235.

[12] a) P. S. Mukherjee, N. Das, P. J. Stang, *J. Org. Chem.* **2004**, *69*, 3526–3529; b) M. D. Ward, *Chem. Commun.* **2009**, 4487–4499; c) V. K. Jain, L. Jain, *Coord. Chem. Rev.* **2010**, *254*, 2848–2903; d) M. Yoshizawa, M. Fujita, *Bull. Chem. Soc. Jpn.* **2010**, *83*, 609–618; e) R. Chakrabarty, P. S. Mukherjee, P. J. Stang, *Chem. Rev.* **2011**, *111*, 6810–6918; f) Y. Inokuma, M. Kawano, M. Fujita, *Nat. Chem.* **2011**, *3*, 349–358; g) H. Amouri, C. Desmarets, J. Moussa, *Chem. Rev.* **2012**, *112*, 2015–2041; h) N. B. Debata, D. Tripathy, D. K. Chand, *Coord. Chem. Rev.* **2012**, *256*, 1831–1945.

[13] a) J. B. Pollock, T. R. Cook, P. J. Stang, *J. Am. Chem. Soc.* **2012**, *134*, 10607–10620; b) K. Uehara, T. Oishi, T. Hirose, N. Mizuno, *Inorg. Chem.* **2013**, *52*, 11200–11209; c) Q.-F. Sun, S. Sato, M. Fujita, *Angew. Chem. Int. Ed.* **2014**, *53*, 13510–13513; *Angew. Chem.* **2014**, *126*, 13728–13731.

[14] a) S. Grimme, *Chem. Eur. J.* **2004**, *10*, 3423–3429; b) S. M. Bachrach, *J. Phys. Chem. A* **2011**, *115*, 2396–2401; c) H. Dodziuk, S. Szymański, J. Jaźwiński, M. Ostrowski, T. B. Demissie, K. Ruud, P. Kuś, H. Hopf, S.-T. Lin, *J. Phys. Chem. A* **2011**, *115*, 10638–10649; d) H. Wolf, D. Leusser, M. R. V. Jørgensen, R. Herbst-Irmer, Y.-S. Chen, E.-W. Scheidt, W. Scherer, B. B. Iversen, D. Stalke, *Chem. Eur. J.* **2014**, *20*, 7048–7053.

[15] J. B. Moffat, *Chem. Phys. Lett.* **1978**, *55*, 125–130.

[16] a) P. Jacopozzi, E. Dalcanale, *Angew. Chem. Int. Ed. Engl.* **1997**, *36*, 613–615; *Angew. Chem.* **1997**, *109*, 665–667; b) A. Mayr, L.-F. Mao, *Inorg. Chem.* **1998**, *37*, 5776–5780; c) F. Fochi, P. Jacopozzi, E. Wegelius, K. Rissanen, P. Cozzini, E. Marastoni, E. Fisicaro, P. Manini, R. Fokkens, E. Dalcanale, *J. Am. Chem. Soc.* **2001**, *123*, 7539–7552; d) R. W. Date, E. F. Iglesias, K. E. Rowe, J. M. Elliott, D. W. Bruce, *Dalton Trans.* **2003**, 1914–1931; e) D. Zuccaccia, L. Pirondini, R. Pinalli, E. Dalcanale, A. Macchioni, *J. Am. Chem. Soc.* **2005**, *127*, 7025–7032; f) A. Schaly, Y. Rousselin, J.-C. Chambron, E. Aubert, E. Espinosa, *Eur. J. Inorg. Chem.* **2016**, 832–843.

[17] M. L. Kuznetsov, *Russ. Chem. Rev.* **2002**, *71*, 265–282.

[18] L. Bondarenko, I. Dix, H. Hinrichs, H. Hopf, *Synthesis* **2004**, *16*, 2751–2759.

[19] H. Allgeier, M. G. Siegel, R. C. Helgeson, E. Schmidt, D. J. Cram, *J. Am. Chem. Soc.* **1975**, *97*, 3782–3789.

[20] G. Meyer-Eppler, R. Sure, A. Schneider, G. Schnakenburg, S. Grimme, A. Lützen, *J. Org. Chem.* **2014**, *79*, 6679–6687.

[21] C. Bannwarth, S. Grimme, *Comput. Theor. Chem.* **2014**, *1040–1041*, 45–53.

[22] R. W. W. Hooft, L. H. Straver, A. L. Spek, *J. Appl. Crystallogr.* **2008**, *41*, 96–103.

[23] P. J. Stang, D. H. Cao, S. Saito, A. M. Arif, *J. Am. Chem. Soc.* **1995**, *117*, 6273–6283.

[24] L. Avram, Y. Cohen, *Chem. Soc. Rev.* **2015**, *44*, 586–602.

[25] a) E. Engeldinger, D. Armspach, D. Matt, *Angew. Chem. Int. Ed.* **2001**, *40*, 2526–2529; *Angew. Chem.* **2001**, *113*, 2594–2597; b) J. Shearer, H. L. Jackson, D. Schweitzer, D. K. Rittenberg, T. M. Leavy, W. Kaminsky, R. C. Scarrow, J. A. Kovacs, *J. Am. Chem. Soc.* **2002**, *124*, 11417–11428.

[26] Please note that the chloride stems from abundant chloride in the ESI source of the spectrometer.

[27] It should be noted that similar ratios were observed in acetonitrile and acetone and mixtures of those with chlorinated solvents indicating that the self-assembly process and the self-sorting are not too solvent dependent as long as the solvent is somehow polar, because we could not observe the formation of discrete aggregates in pure chlorinated solvents like dichloromethane or chloroform (see Supporting Information).

[28] I. Ugi, *Isonitrile Chemistry*, Academic Press, New York, **1971**.

[29] M. Ernzerhof, G. Scuseria, *J. Chem. Phys.* **1999**, *110*, 5029–5036.

[30] F. Weigend, R. Ahlrichs, *Phys. Chem. Chem. Phys.* **2005**, *7*, 3297–3305.

[31] E. Caldeweyher, S. Ehlert, A. Hansen, H. Neugebauer, S. Spicher, C. Bannwarth, S. Grimme, *J. Chem. Phys.* **2019**, *150*, 154122.

[32] a) A. Klamt, *J. Phys. Chem.* **1995**, *99*, 2224–2235; b) A. Klamt, V. Jonas, T. Bürger, J. C. Lohrenz, *J. Phys. Chem. A* **1998**, *102*, 5074–5085.

[33] S. Grimme, J. G. Brandenburg, C. Bannwarth, A. Hansen, *J. Chem. Phys.* **2015**, *143*, 054107.

[34] C. Bannwarth, S. Ehlert, S. Grimme, *J. Chem. Theory Comput.* **2019**, *15*, 1652–1671.

[35] a) A. Mayr, J. Guo, *Inorg. Chem.* **1999**, *38*, 921–928; b) N. Koiso, Y. Kitagawa, T. Nakanishi, K. Fushimi, Y. Hasegawa, *Inorg. Chem.* **2017**, *56*, 5741–5747.

[36] a) H. Konaka, L. P. Wu, M. Munakata, T. Kuroda-Sowa, M. Maekawa, Y. Suenaga, *Inorg. Chem.* **2003**, *42*, 1928–1934; b) E. D. Genuis, J. A. Kelly, M. Patel, R. McDonald, M. J. Ferguson, G. Greidanus-Strom, *Inorg. Chem.* **2008**, *47*, 6184–6194; c) P. Niranjana, A. Pati, S. K. Porwal, V. Ramkumar, S. J. Gharpure, D. K. Chand, *CrystEngComm* **2013**, *15*, 9623–9633; d) Z. Wang, S. Begum, H. Krautscheid, *Cryst. Growth Des.* **2016**, *16*, 5836–5842.

[37] a) L. Brunsveld, B. J. B. Folmer, E. W. Meijer, R. P. Sijbesma, *Chem. Rev.* **2001**, *101*, 4071–4098;; b) R. Dobrawa, F. Würthner, *J. Polym. Sci. Polym. Chem.* **2005**, *43*, 4981–4995; c) E. Yashima, K. Maeda, Y. Furusho, *Acc. Chem. Res.* **2008**, *41*, 1166–1180;; d) L. Yang, X. Tan, Z. Wang, X. Zhang, *Chem. Rev.* **2015**, *115*, 7196–7239; e) E. Yashima, N. Ousaka, D. Taura, K. Shimomura, T. Ikai, K. Maeda, *Chem. Rev.* **2016**, *116*, 13752–13990; f) S. Shanmugaraju, C. S. Hawes, A. J. Savyasachi, S. Blasco, J. A. Kitchen, T. Gunnlaugsson, *Chem. Commun.* **2017**, *53*, 12512–12515.

[38] T. Yanai, D. Tew, N. Handy, *Chem. Phys. Lett.* **2004**, *393*, 51–57.

[39] F. Neese, *WIREs Comput. Mol. Sci.* **2017**, *8*, e1327.

[40] S. Grimme, C. Bannwarth, P. Shushkov, *J. Chem. Theory Comput.* **2017**, *13*, 1989–2009.

[41] a) A. D. Becke, *Phys. Rev. A* **1988**, *38*, 3098–3100; b) C. Lee, W. Yang, R. G. Parr, *Phys. Rev. B* **1988**, *37*, 785–789; c) A. D. Becke, *J. Chem. Phys.* **1993**, *98*, 1372–1377.

[42] TURBOMOLE 7.2.1 2017 a development of University of Karlsruhe and Forschungszentrum Karlsruhe GmbH, 1989–2007, TURBOMOLE GmbH, since 2007, available from http//www.turbomole.com.

[43] https://www.chemie.uni-bonn.de/pctc/mulliken-center/software/stda/stda.

[44] A. V. Marenich, C. J. Cramer, D. G. Truhlar, *J. Phys. Chem. B* **2009**, *113*, 6378–6396.

[45] S. Grimme, *Chem. Eur. J.* **2012**, *18*, 9955–9964.

[46] a) A. D. Becke, *J. Chem. Phys.* **1993**, *98*, 5648–5652; b) P. J. Stephens, F. J. Devlin, C. F. Chabalowski, and M. J. Frisch, *J. Phys. Chem.* **1994**, *98*, 11623–11627.

[47] K. Eichkorn, O. Treutler, H. Öhm, M. Häser, R. Ahlrichs, *Chem. Phys. Lett.* **1995**, *242*, 652–660.

[48] F. Weigend, *Phys. Chem. Chem. Phys.* **2006**, *8*, 1057–1065.

[49] a) COSMOtherm, release 1601, COSMOlogic GmbH & Co KG, http://www.cosmologic.de; b) "Fast solvent screening via quantum chemistry: COSMO-RS approach": F. Eckert, A. Klamt, *AIChE J.* **2002**, *48*, 369–385.

[50] R. H. Blessing, *Acta. Cryst. A* **1995**, *51*, 33–38.

[51] Rigaku Oxford Diffraction, (2017), CrysAlisPro Software system, version 1.171.38.43, Rigaku Corporation, Oxford, UK.

[52] G. M. Sheldrick, *Acta Crystallogr. Sect. A* **2015**, *71*, 3–8.

[53] G. M. Sheldrick, *Acta Crystallogr. Sect. C* **2015**, *71*, 3–8.

[54] O. V. Dolomanov, L. J. Bourhis, R. J. Gildea, J. A. K. Howard, H. Puschman, *J. Appl. Crystallogr.* **2009**, *42*, 339–341.

[55] L. J. Farrugia, *J. Appl. Crystallogr.* **2012**, *45*, 849–854.